Estimation of radio refractivity using a multiple angle clutter model

Ali Karimian,[1] Caglar Yardim,[1] William S. Hodgkiss,[1] Peter Gerstoft,[1] and Amalia E. Barrios[2]

Received 4 March 2011; revised 16 February 2012; accepted 21 February 2012; published 10 April 2012.

[1] The common occurrence of a marine boundary layer in coastal regions can affect radio wave propagation significantly. Refractivity from clutter (RFC) techniques are aimed at estimating the refractivity profile of the ambient environment based on the received radar clutter. While most previous RFC work has not considered the dependence of RFC inversions on a variable grazing angle, this study investigates incorporation of the grazing angle information into the clutter model. A newly proposed clutter model based on multiple incident angles at each range is used here. The inversion performance of the multiple angle clutter model is compared to that of other models. Synthetic examples of a range-independent surface-based duct and a range-dependent evaporation duct are investigated for a S-band radar. Finally, a comparison of inversions on one set of experimental measurements from the SPANDAR 1998 data set is provided, using single and multiple grazing angle clutter models, and the previously used model based on grazing angle independent sea surface reflectivity.

Citation: Karimian, A., C. Yardim, W. S. Hodgkiss, P. Gerstoft, and A. E. Barrios (2012), Estimation of radio refractivity using a multiple angle clutter model, *Radio Sci.*, *47*, RS0M07, doi:10.1029/2011RS004701.

1. Introduction

[2] Lower atmospheric ducts over the ocean are common in many maritime regions of the world. These non-standard conditions create effects such as significant variations in the maximum operational radar range, creation of radar fades where the radar performance is reduced, and increased sea clutter [*Skolnik*, 2008]. Atmospheric ducts are more common in hot and humid regions of the world. The Persian Gulf, the Mediterranean and California coasts are examples of such regions with common formation of a ducting layer above the sea surface [*Yardim et al.*, 2009].

[3] Surface-based ducts appear almost 25% of the time off the coast of South California and 50% in the Persian Gulf [*Patterson*, 1992]. Efforts in remote sensing and numerical weather prediction have been directed toward a better estimation of the refractivity profile in the lower atmosphere (less than 500 m above the sea surface) [*Rogers*, 1997; *LeFurjah et al.*, 2010]. The atmospheric refractivity profile is often measured by direct sensing of the environment. Rocketsondes and radiosondes typically are used for in situ sampling of the surface layer [*Rowland et al.*, 1996]. Lidar [*Willitsford and Philbrick*, 2005] and GPS signals [*Lowry et al.*, 2002] also have been used to measure the vertical refractivity profile.

[4] A more recent approach, refractivity from clutter (RFC), uses the radar return signals to estimate the ambient environment refractivity profile [*Rogers et al.*, 2000; *Gerstoft et al.*, 2003; *Yardim et al.*, 2006; *Vasudevan et al.*, 2007; *Douvenot et al.*, 2010; *Karimian et al.*, 2011]. This approach makes tracking of spatial and temporal changes in the environment possible [*Yardim et al.*, 2008].

[5] Most previous RFC studies have considered a grazing angle-independent clutter model. This model is a consequence of neglecting the effect of a variable grazing angle on the clutter power at low angles [*Gerstoft et al.*, 2003; *Douvenot and Fabbro*, 2010], or the convergence of angles at far ranges. Convergence of the grazing angle at far ranges is valid for a range-independent evaporation duct [*Rogers et al.*, 2000; *Yardim et al.*, 2009].

[6] Grazing angle is range-dependent in ducted environments. In addition, multiple angles of arrival at each range typically are present in strong surface-based ducts (e.g. see Figure 1c) [*Karimian et al.*, 2011; A. Karimian et al., Multiple grazing angle sea clutter modeling, submitted to *IEEE Transactions on Antennas and Propagation*, 2012]. Thus, neglecting changes of the grazing angle along the propagation path, or assuming single path propagation does not yield a realistic clutter model in ducted environments. *Rogers et al.* [2005] and *Vasudevan et al.* [2007] have considered horizontal variability of the sea surface reflectivity, albeit considering it as a random process.

[7] The present study uses two approaches to include the grazing angle information: a range-dependent single angle clutter model that is based on the maximum grazing angle at each range, and a range-dependent multiple angle clutter model that is based on all angles of arrival. The worst

[1]Marine Physical Laboratory, Scripps Institution of Oceanography, University of California, San Diego, USA.
[2]Atmospheric Propagation Branch, Space and Naval Warfare Systems Center, San Diego, California, USA.

0048-6604/12/2011RS004701

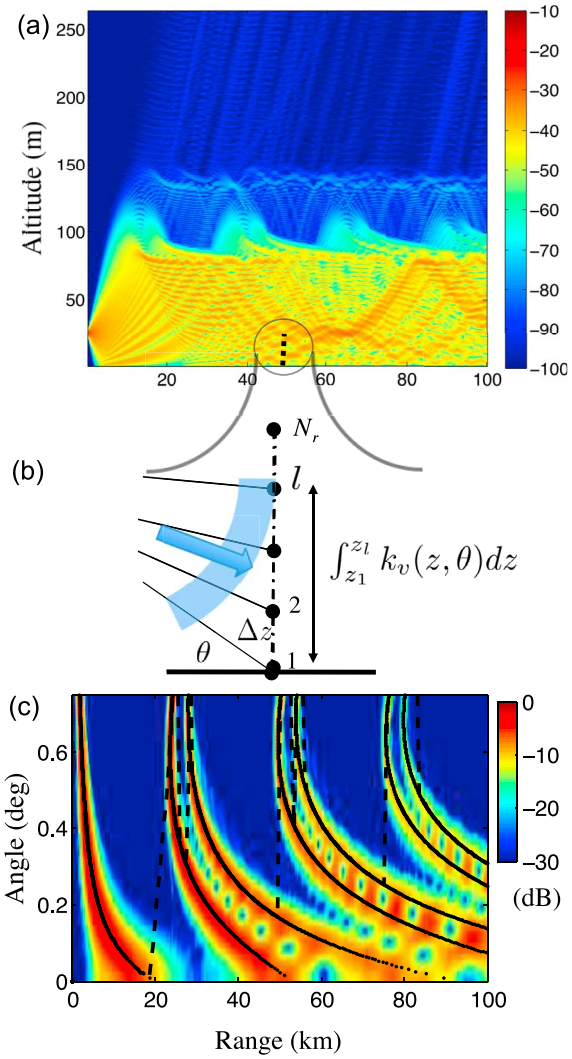

Figure 1. (a) Power $|u|^2$ (dB) from the parabolic equation (PE) propagation model in an arbitrary surface-based duct similar to the profile of Figure 2c. (b) Geometry of the line array used for the estimation of grazing angles at each range for curved wave spectral estimation. (c) Angular spectral power (contour plot), grazing angle from ray tracing (solid), the maximum angle from ray tracing (dashed).

case clutter in maritime environments can be calculated by considering the maximum grazing angle at each location [*Barrios*, 2002; *Dockery et al.*, 2007]. However, this model is not appropriate for RFC applications where a more realistic model for the expected clutter is required. The multiple angle clutter model incorporates all incident wavefronts and weights them proportional to their relative powers (Karimian et al., submitted manuscript, 2012).

2. Sea Clutter at Low Grazing Angles

[8] Radars operating in maritime environments encounter a back-scattered field from the sea surface which depends on the refractivity profile of the environment known as the M-profile. This dependence makes inference on the refractivity profile from the observed clutter possible [*Gerstoft et al.*, 2003]. The expected clutter at range r is expressed as [*Dockery*, 1990]:

$$P_c(r) = \frac{P_t G^2 \lambda^2 \theta_B c \tau \sigma_0 \sec(\theta) F^4(r)}{2(4\pi r)^3 L}, \quad (1)$$

where P_t is the transmitter power, G is the antenna gain, λ is the wavelength, θ_B is the antenna pattern azimuthal beam width, c is the propagation speed, τ is the pulse width, σ_0 is the sea surface reflectivity per unit area, θ is the grazing angle at range r, F is the propagation factor, and L is the total assumed system losses.

[9] The pattern propagation factor F is defined as the ratio of the magnitude of the electric field at a given point under specified conditions to the magnitude of the electric field under free-space conditions with the beam of the transmitter directed toward the point in question [*Kerr*, 1951]: $F(r) = \frac{|E(r)|}{|E_{fs}(r)|}$.

[10] A review of the three models of clutter power that are used in this study is provided below.

2.1. Grazing Angle Independent Clutter Model

[11] The dependence of the sea surface reflectivity on the grazing angle has not been included in most previous RFC studies [*Gerstoft et al.*, 2003; *Douvenot et al.*, 2010]. This assumption results in a range-independent sea surface reflectivity term in the clutter power equation. The sec(θ) term also is a weak function of θ at low grazing angles. Thus, normalizing the clutter power with reference to the power at range r_o yields the approximation:

$$\frac{P_c(r)}{P_c(r_o)} \simeq \left(\frac{r_o}{r}\right)^3 \frac{F^4(r)}{F^4(r_o)}. \quad (2)$$

[12] The propagation factor F can be obtained from a parabolic equation (PE) code [*Barrios*, 1994]. The assumption of an angle-independent sea surface reflectivity is valid where grazing angle does not significantly vary with range.

2.2. Range-Dependent Single Grazing Angle Clutter

[13] The clutter power typically is estimated based on a single grazing angle of an incident wavefront at each range. The grazing angle can be estimated from ray theory [*Barrios*, 2002] or from angular spectral estimation techniques, such as MUSIC, that calculate the angle of arrival [*Dockery*, 1988]. Both of these methods might yield several grazing angles at each range. Usage of the maximum grazing angle at each location leads to the worst case clutter power. This is a conservative estimate of the expected clutter power that is used in radar performance analysis. However, ray tracing has its own limitations. There are surface locations that rays do not reach, requiring interpolation or extrapolation of grazing angles at those ranges.

[14] The sea surface reflectivity σ_0 is dependent on the grazing angle θ. In practice it is common to use the semi-empirical sea surface reflectivity model from the Georgia Institute of Technology (GIT) [*Horst et al.*, 1978]. GIT is based on fitting the experimental measured average surface reflectivity to a function of polarization, radar frequency,

grazing angle, wind speed and radar look direction [*Dockery*, 1990]. It is assumed that the GIT model is based on measurements obtained under standard atmospheric conditions. This model also depends on a single grazing angle. *Reilly and Dockery* [1988] modified the GIT model to take into account the effects of non-standard ducting conditions on sea clutter. They divided the GIT surface reflectivity by the standard atmosphere propagation factor to remove the standard atmospheric effect on the measurements. Derivation of surface reflectivity models at low grazing angles continue to be an active field of research [*Gregers-Hansen and Mital*, 2009]. Using the modified GIT sea surface reflectivity model, the clutter power equation is obtained as:

$$P_c(r) = \frac{P_t G^2 \lambda^2 \theta_B c\tau \sigma_{0,GIT}(r) \sec(\theta) F^4(r)}{2(4\pi r)^3 L F_{std}^4(r')}, \quad (3)$$

where $F_{std}^4(r')$ is the two-way propagation factor of a standard atmosphere ($\frac{dM}{dh} = 0.118$ M-units/m) at range r' with the same wind speed and an isotropic antenna. r' is the range corresponding to the grazing angle θ in the standard atmosphere with an identical radar height and an isotropic antenna.

2.3. Range-Dependent Multiple Grazing Angle Clutter

[15] Angular spectral estimation techniques find the incident power distribution versus grazing angle at each range. The elements of the vertical synthetic array (Figure 1a) are formed from the complex field u at each range obtained from the FFT bins of the electromagnetic parabolic equation (PE) propagation model. For Cartesian coordinates [*Levy*, 2000]:

$$u(x,z) = e^{-jkx}\psi(x,z), \quad (4)$$

where x is the horizontal Cartesian range, z is the altitude, and k is the wave number. ψ is the tangential electric field E_y for horizontal polarization, and the tangential magnetic field H_y for vertical polarization.

[16] A multiple angle clutter model based on curved wave spectral estimation (CWS) (Karimian et al., submitted manuscript, 2012) is considered in this work. CWS is a non-plane wave spectral estimation technique based on the Wentzel-Kramers-Brillouin-Jeffreys(WKBJ) approximation to the electromagnetic wave propagation solution. The WKBJ approximation provides a solution in a lossless inhomogeneous medium assuming that the field solution $u(x, z)$ is separable: $u(x, z) = t(x)f(z)$. This approximation requires the vertical wave number $k_v(z)$ to be slowly varying along the coordinate system [*Someda*, 2006]. The latter condition can be simplified in plane wave propagation to the condition that the medium changes slowly with respect to the wavelength. The vertical field $f(z)$ is a summation of multiple pairs of incident and reflected wavefronts. The field due to each pair of wavefronts with angle θ at the surface in the WKBJ approximation is expressed as [*Someda*, 2006]:

$$h(z,\theta) = \frac{A_i}{\sqrt{k_v(z,\theta)}} e^{+j\int_{z_1}^{z} k_v(z,\theta)dz} + \frac{A_r}{\sqrt{k_v(z,\theta)}} e^{-j\int_{z_1}^{z} k_v(z,\theta)dz}, \quad (5)$$

where A_i and A_r are constants of the incident and forward reflected waves, and z_1 denotes the sea surface. A_i and A_r are related by $A_r = \Gamma A_i$ with Γ the reflection coefficient. Assuming $\Gamma = -1$, (5) is simplified:

$$h(z,\theta) = \frac{A_i}{\sqrt{k_v(z,\theta)}} \left(e^{+j\int_{z_1}^{z} k_v(z,\theta)dz} - e^{-j\int_{z_1}^{z} k_v(z,\theta)dz} \right). \quad (6)$$

[17] The geometry of CWS is shown in Figure 1b. Spatial samples of the PE field are used along a vertical line array. CWS matches to the phase variations of different array elements based on the WKBJ solution. An inherent assumption in CWS is that the curvature of wavefronts is only due to an inhomogeneous medium.

[18] Let the medium have a stratified structure with the modified atmospheric refractive index $n_{mod}(z)$ at each range r and height z. The modified refractive index is obtained by $n_{mod}(z) = n_r(z) + \frac{z}{r_e}$ from the atmospheric refractive index $n_r(z)$ and earth radius r_e, which is a flat earth approximation to the spherical propagation problem.

[19] The vertical wave number k_v is a function of the wave number k, the horizontal wave number k_h, and gazing angle θ. Let ω denote the angular frequency, and c_0 the wave speed in a vacuum. Applying Snell's law for k_h yields:

$$\begin{aligned} k_v(z,\theta) &= \sqrt{k^2(z) - k_h^2(z,\theta)} \\ &= \frac{\omega}{c_0}\sqrt{n_{\mathrm{mod}}^2(z) - n_{\mathrm{mod}}^2(z_1)\ \cos^2\theta}. \end{aligned} \quad (7)$$

With k_v real, the phase difference between z_1 and z_l is obtained by integration of k_v along the vertical line joining the aforementioned points:

$$\phi_l(\theta) = \int_{z_1}^{z_l} k_v(z,\theta)dz. \quad (8)$$

[20] The CWS output in direction θ is obtained by matching to the phase variations of array elements for a pair of incident and reflected wavefronts with angle θ, expressed in (6):

$$\begin{aligned} B_{\mathrm{CWS}}(\theta) &= \sum_{l=1}^{N_r} w_l u_l \left(e^{-j\phi_l} - e^{j\phi_l}\right) \\ &= -2j\sum_{l=1}^{N_r} w_l u_l \sin\left(\int_{z_1}^{z_l} k_v(z,\theta)dz\right), \end{aligned} \quad (9)$$

where u_l is the PE field at the lth element of the array and $\{w_l\}$ are the weighting coefficients of the array, here half a Hamming window. This is equivalent to using a Hamming window on a double size array that covers the incident and reflected wavefronts separately (Karimian et al., submitted manuscript, 2012). N_r is the index of the highest array element with $k_v \geq 0$.

[21] Figure 1c shows an example that exhibits variable grazing angles. Figures 1a and 1c are based on computations from an environment with a refractivity structure similar to Figure 2c. Figure 1c shows that in a range-independent

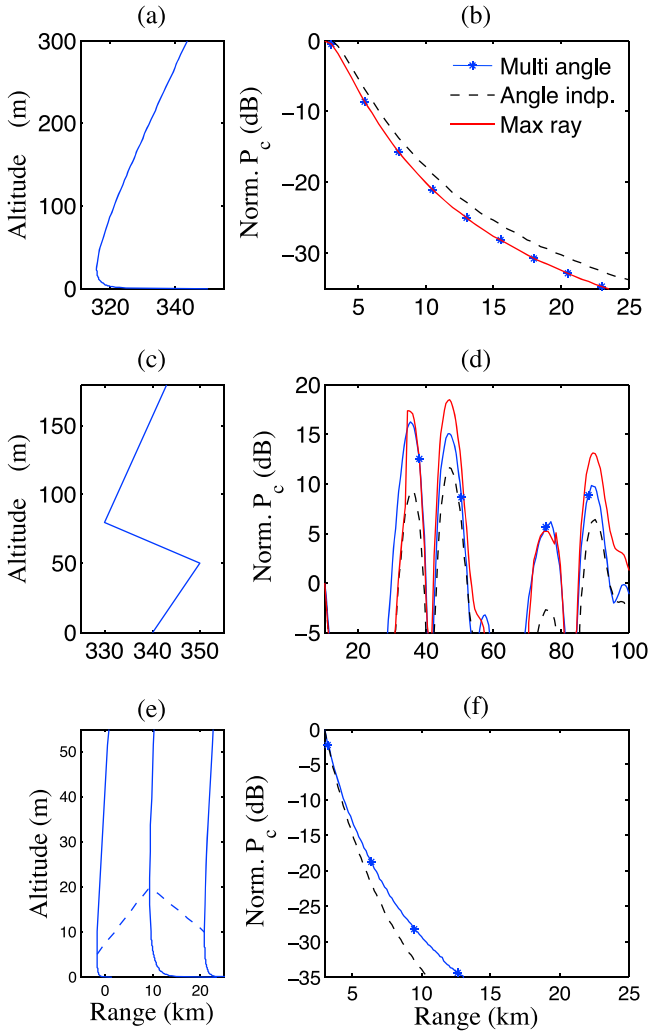

Figure 2. (a, c, e) Refractivity profile and (b, d, f) corresponding clutter power at 3 GHz using various clutter models: multiple grazing angle, angle independent, and maximum angle from ray tracing.

surface-based duct, constant or single grazing angle assumptions are not necessarily valid. Also, most practical situations include a range varying refractivity profile [*Gerstoft et al.*, 2003] where a range-independent grazing angle assumption is no longer valid. Inversion of a range-dependent evaporation duct is studied in section 3.2.

[22] The angular spectral power $\gamma(\theta) = |B_{\mathrm{CWS}}(\theta)|^2$ is obtained from (9). $\gamma(\theta)$ can be used to decompose the total power into the power arriving from different directions. The multiple angle clutter model is obtained as:

$$P_c(r) = \frac{\alpha_r F^4(r)}{\int_\theta \gamma(\theta) d\theta} \int_\theta \frac{\sigma_{0,GIT}(\theta)\sec(\theta)\gamma(\theta)}{F^4_{std}(\theta)} d\theta, \qquad (10)$$

where $\alpha_r = \frac{P_t G^2 \lambda^2 \theta_\beta c\tau}{2(4\pi r)^3 L}$ includes all θ independent terms.

[23] The multiple angle clutter model (10) can be visualized by assuming a discrete set of N_θ grazing angles. Using spectral estimation, incident power at each range can be decomposed into its angular components $\{\gamma(\theta_i)\}_{i=1}^{N_\theta}$. Consider the weighted propagation factor associated with grazing angle θ_i to be defined by:

$$F_i^2(r) \triangleq F^2(r) \frac{\gamma(\theta_i)}{\sum_{n=1}^{N_\theta} \gamma(\theta_n)}. \qquad (11)$$

Incident power is assumed to be back-scattered uniformly. Due to reciprocity, back-scattered angles received by the radar are identical to the incident angles at the same range. Thus, the total clutter power is:

$$P_c(r) = \sum_{i=1}^{N_\theta} \alpha_r F_i^2(r)\sigma_0(\theta_i)\sec(\theta_i) \sum_{j=1}^{N_\theta} F_j^2(r)$$
$$= \sum_{i=1}^{N_\theta} \alpha_r F^2(r) F_i^2(r)\sigma_0(\theta_i)\sec(\theta_i). \qquad (12)$$

Substituting (11) into (12) yields the discrete form of (10). Here, we have assumed different propagation paths to be uncorrelated.

[24] Figure 2 compares clutter power obtained from the previously mentioned models. Figures 2a, 2c, and 2e show the refractivity profiles of the modeled environment, and Figures 2b, 2d, and 2f show the corresponding clutter power at 3 GHz, vertical polarization, antenna beam width of 0.4°, antenna height of 15 m and wind speed of 5 m/s. All clutter power plots are normalized with reference to the starting range (10 km for the surface-based duct example and 3 km for evaporation duct examples).

[25] Figure 2a shows a range-independent evaporation duct with duct height of 24 m. Differences between the fall-off rates of angle dependent and independent models are due to rapid variations of the grazing angle in the vicinity of the radar. Most previous RFC studies considered the clutter power at ranges where grazing angle does not vary significantly with range. For evaporation ducts, this region is shown in Figure 1 of *Yardim et al.* [2009]. However, this usually means avoiding the region in the vicinity of the radar where clutter to noise ratio is high. Figure 2 shows a surface-based duct. Its corresponding clutter power obtained from the maximum angle of ray tracing shows larger dynamic range and discontinuities at boundaries of ray theory shadow zones. Figure 2e shows a range-dependent evaporation duct which is discussed further in section 3.2. The modeled clutter power, assuming angle dependent sea surface reflectivity, results in different clutter power than when using angle independent sea surface reflectivity. The multiple angle and maximum angle from ray tracing clutter power results are identical. The latter is due to the single angle nature of propagation in an evaporation duct.

3. Performance Analysis for RFC Estimation

[26] Refractivity from clutter techniques find the best refractivity profile that matches the observed clutter. The expected clutter power of each candidate profile is computed and an objective function is formed that quantifies the distance between the observed and the modeled clutter. The candidate profile that yields the minimum objective function is declared as the best match. Previous RFC studies have considered the sum of the squared errors, the l_2 norm, as the

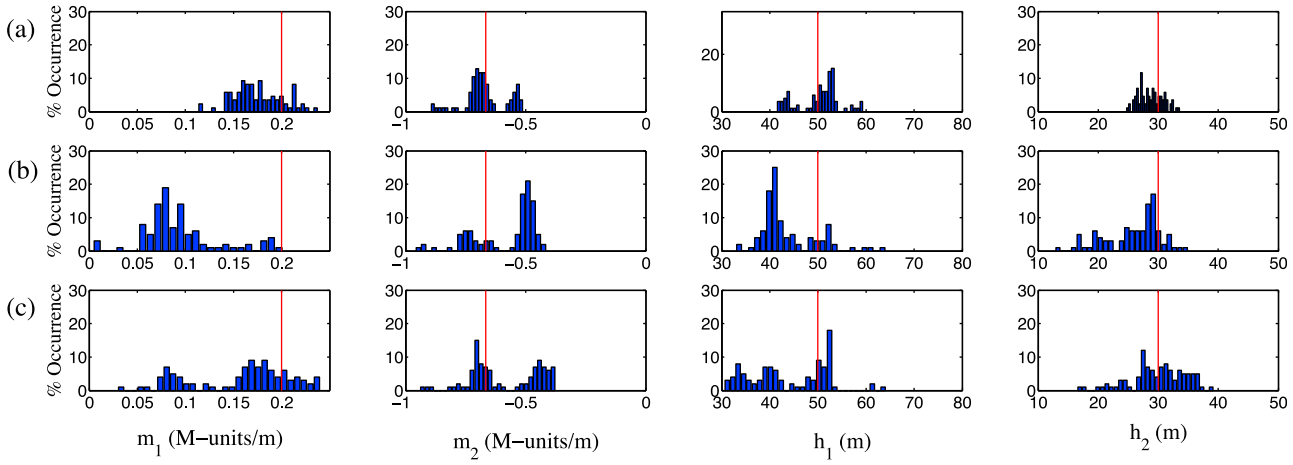

Figure 3. Inverted surface based duct parameters using various clutter models: (a) multiple angle, (b) maximum angle from ray tracing, and (c) angle-independent. The simulated clutter power is modeled by the multi angle clutter model and include random components of the sea surface reflectivity and noise floor in the receiver. Vertical lines are the actual parameters of this synthetic example.

objective function [*Gerstoft et al.*, 2003; *Vasudevan et al.*, 2007; *Yardim et al.*, 2009]. The main purpose of this section is to analyze how different clutter models affect the RFC model parameters.

3.1. Surface-Based Ducts

[27] Surface-based ducts typically are due to the advection of warm and dry coastal air to the sea. These ducts are less common than evaporation ducts but their effect is more prominent on radar returns [*Skolnik*, 2008]. Here, the M-profile of a surface-based duct is approximated by a tri-linear function:

$$M(z) = M_0 + \begin{cases} m_1 z & z \le h_1 \\ m_1 h_1 + m_2 (z - h_1) & h_1 \le z \le h_1 + h_2 \\ m_1 h_1 + m_2 h_2 & h_1 + h_2 \le z \\ +m_0 (z - h_1 - h_2) & \end{cases} \quad (13)$$

[28] A genetic algorithm is used to invert for the parameters m_1, m_2, h_1, h_2 based on observed clutter [*Yardim et al.*, 2007]. m_0 = 0.118 M-units/m is the slope of the standard atmosphere. The specific choice of M_0 (here 320 M-units) does not affect the propagation pattern of electromagnetic waves and does not affect the parameter estimation.

[29] The radar and environmental parameters in this example are: 3 GHz radar frequency, 25 m antenna height, 5 m/s wind speed, antenna beam width of 0.4° and vertical polarization. The surface-duct parameters are identical to those of Figure 2c. The results of Figures 3a–3c are obtained by running 200 inversions on the modeled clutter.

[30] Two random components in the observed clutter power are modeled here: variations of sea surface reflectivity and noise at the receiver. The selection of sea surface reflectivity statistics for RFC applications depends on the wind speed and direction, grazing angle, polarization and the radar range resolution [*Long*, 2000]. Low grazing angle results in complex scattering mechanisms, such as shadowing caused by sea swells and diffraction over the wave edges. These factors increase the spikiness of the sea surface clutter [*Ward et al.*, 2005]. On the other hand, decreasing the radar resolution increases the number of random scatters inside each range bin, which in turn reduces the spiky behavior of the sea surface reflectivity [*Skolnik*, 2008]. The effect of different distributions on clutter modeling and RFC is investigated by *Yardim et al.* [2009]. The receiver noise floor is another source of randomness that affects the observed radar clutter [*Rogers et al.*, 2000].

[31] Here, variations of the surface reflectivity from GIT is modeled using a lognormal distribution with zero mean and 3 dB standard deviation Gaussian in the logarithmic domain. The additive receiver noise is modeled by a Gaussian distribution over the complex field [*Yardim et al.*, 2009]. Clutter power is normalized at the range of 10 km. Clutter to noise ratio at that range (CNR_{10km}) is taken as 40 dB. The observed clutter power is obtained from the multiple grazing angle clutter model.

[32] Results in Figure 3a are distributed around the original parameters as expected, since both simulated clutter and inversion algorithm use the same clutter model. The plots in Figure 3b show that using a single angle clutter model obtained from the maximum angle from ray tracing yields a biased estimation. The bias of the estimated parameters is especially clear in the first slope (m_1) and the second height (h_2) of the trilinear model in this example. Using the maximum angle of arrival is common in the calculation of the worst case clutter [*Barrios*, 2002; *Dockery et al.*, 2007], but is not appropriate for RFC applications. The plots in Figure 3c are obtained by inversion using a grazing angle independent clutter model, which has been used in previous RFC studies. Some bias is observed in RFC using the latter method, but the bias is less than using a clutter model with the maximum arrival angle.

[33] The propagation factor of the profile used in the simulation of Figure 3 is plotted in Figure 4a. The propagation factors and electric fields are obtained using the parabolic equation (PE) code in the Advanced Propagation Model [*Barrios*, 2002]. The differences between the propagation factors of the inverted profiles and the original profile

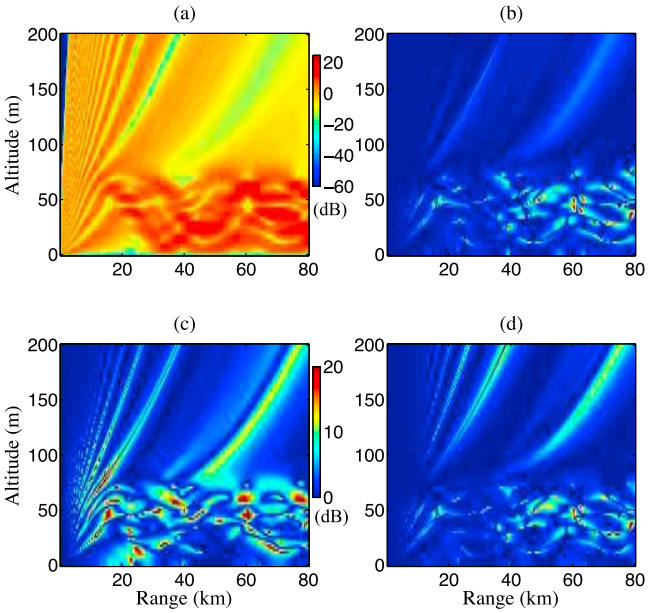

Figure 4. (a) Propagation factor (dB) corresponding to the refractivity profile in Figure 2c. (b–d) The difference between the propagation factors of the original profile and inversion of noisy signals using multiple angle, maximum angle from ray tracing, and angle-independent clutter models respectively. The color scale is identical in Figures 4b–4d. Profile parameters are obtained from the distribution peaks in Figure 3.

are compared in Figures 4b–4d. The assumption of an angle independent sea surface reflectivity (Figure 4d) yields 1.8 dB average error in the propagation factor of the inverted profile in the ducted regions, while inversion using the single angle clutter from maximum arrival angle produces a larger average error of 3.6 dB.

3.2. Range-Dependent Evaporation Duct

[34] Evaporation ducts are the most common types of non-standard atmospheric phenomena in maritime environments. The Paulus-Jeske model provides a relationship between modified refractivity M, altitude z and duct height h_d [*Paulus*, 1985]. Assuming equal temperature of the sea surface and air layer boundary simplifies the Paulus-Jeske model [*Rogers et al.*, 2000]:

$$M(z) = M_0 + c_0\left(z - h_d \ln\frac{z+h_0}{h_0}\right), \qquad (14)$$

where M_0 is the base refractivity usually taken as 350 M-units, c_0 = 0.13 M-unit/m is the linear slope of the refractivity and h_0 is the roughness factor taken as 1.5×10^{-4} m.

[35] This section considers a range-dependent evaporation duct with duct heights of 5, 20 and 10 m at ranges of 0, 12.5 and 25 km respectively (shown in Figure 2e). Duct heights in-between are linearly interpolated. The simulated clutter power is used to invert for the duct heights using the multiple angle and the angle-independent clutter models. The histograms of inverted duct heights are shown in Figure 5 using 30 inversions. The radar in this synthetic example operates at 3 GHz and located at 12 m above the sea surface. The bias in the inversion results of the angle-independent clutter model exemplifies that the latter model is not a good candidate for inverting range-dependent environments.

3.3. SPANDAR 1998 Data Set

[36] All three clutter models in this study are compared using the SPANDAR 1998 data. Refractivity profile measurements and radar returns were recorded in Wallops Island, Virginia, April 1998 [*Rogers et al.*, 2000; *Gerstoft et al.*, 2003]. The clutter signals were measured using the Space Range Radar (SPANDAR) with operational frequency of 2.84 GHz, horizontal beam width of 0.4°, elevation angle of 0, antenna height of 30.78 m, and vertical polarization. The refractivity profiles of the environment were measured using an instrumented helicopter provided by the Johns Hopkins University Applied Physics Laboratory. The helicopter flew in and out along the 150° radial from a point 4 km due east of the SPANDAR in a saw-tooth pattern with each transect lasting 30 minutes. Only the first 60 km of clutter power is used to invert for the refractivity profile to maintain a high CNR and avoid high spatial variations of the refractivity index with range.

[37] The range-dependent refractivity profile measured by the helicopter is shown in Figure 7a.This profile corresponds to the measurement on April 2, 1998 from 13:19:14 to 13:49:00 (Run 07). The spatial variations of the M-profile are small in the 0–55 km range. Thus, RFC results from the corresponding clutter observations are compared to the average of the measured M-profiles in that range interval. Note that although measurements show slow range variations, the inversions are based on a range-independent profile.

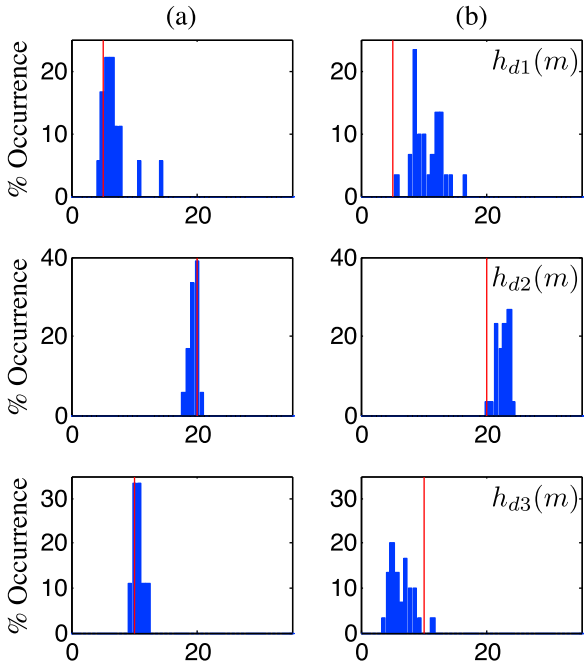

Figure 5. Inverted range-dependent evaporation duct height parameters using clutter models: (a) multiple angle and (b) angle-independent. Vertical lines denote the actual parameters of this synthetic example. Each row corresponds to one of the refractivity profile parameters.

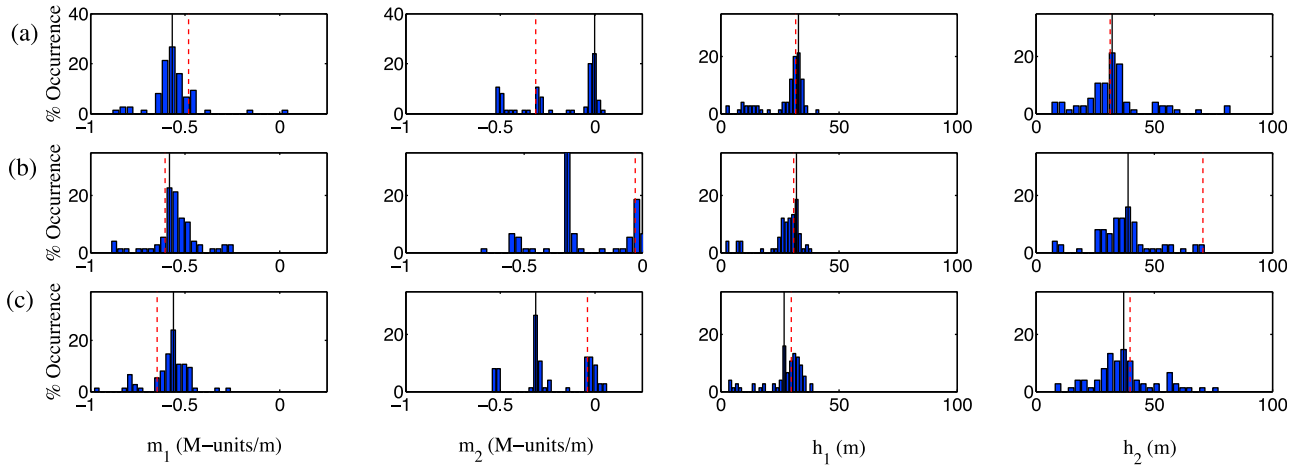

Figure 6. Histograms of estimated trilinear function parameters for the SPANDAR data set, Run 07, along azimuth 145–155°. The peaks of parameter distribution (solid lines) are used in Figure 7. Inversions use different clutter models: (a) multiple angle, (b) maximum angle from ray tracing, (c) angle-independent. Dashed lines show inverted parameters only using the clutter at 150°.

[38] Clutter power recorded from the SPANDAR between azimuth 145–155° are used for estimation of the trilinear function representing a surface based duct, since the clutter pattern and the two duct parameters m_1 and h_1 are rather stationary in this interval [*Yardim et al.*, 2008]. Histograms of estimated parameters using three different clutter models are plotted in Figure 6. The peaks of the parameter distributions (solid lines in Figure 6) are used in Figure 7 to

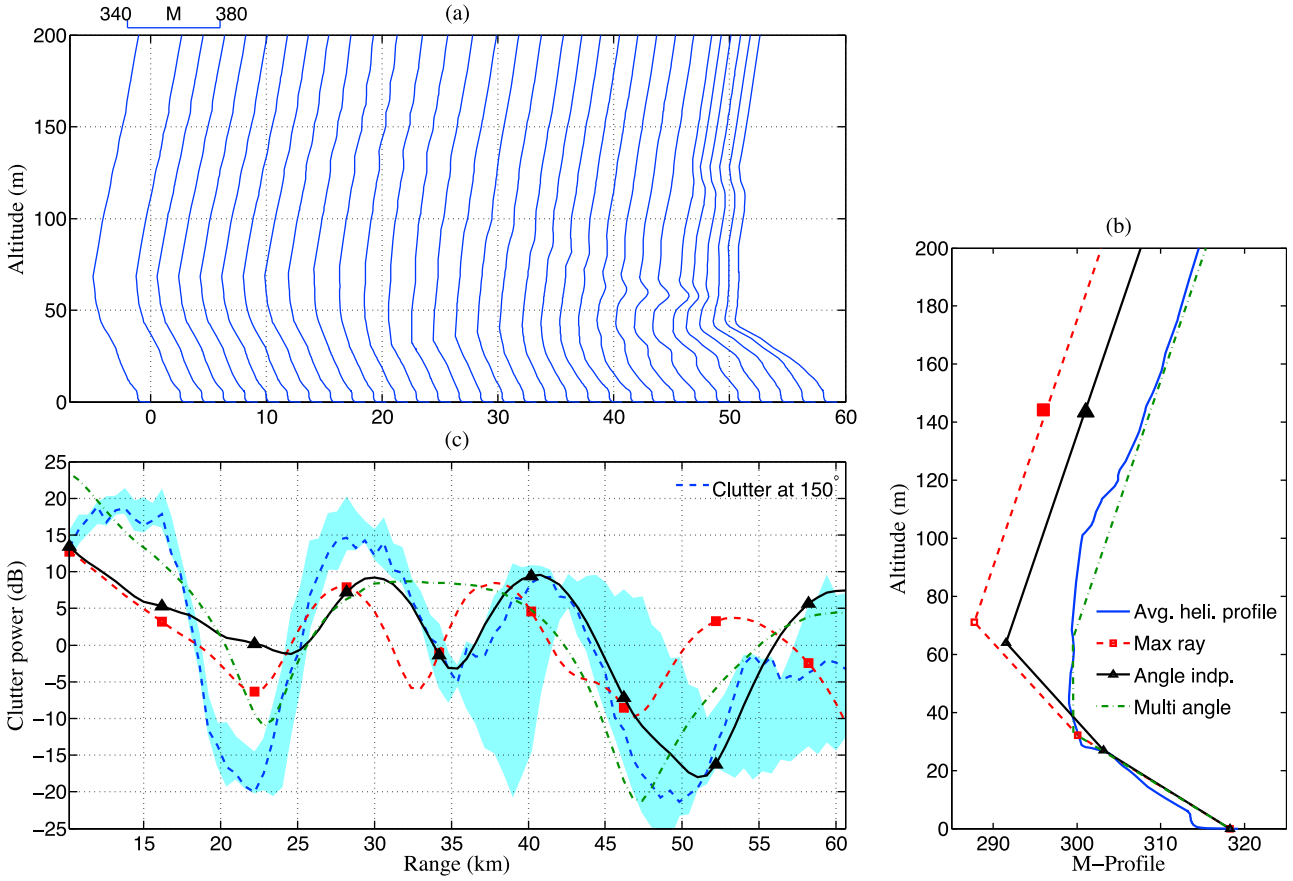

Figure 7. (a) Refractivity profile along the 150° azimuthal line. (b) Average of the first 55 km of measured refractivity profiles compared to the estimated profiles from RFC. Trilinear function parameters are obtained from Figure 6. (c) Observed clutter at 150° azimuth and modeled clutters based on inverted profiles. The shaded area shows the variation of clutter power between 145–155° used in RFC.

represent the estimated refractivity profiles and their clutter powers. The dashed lines in Figure 6 are the inverted parameters using only the clutter power at 150° azimuth. The distribution of inverted parameters for m_1 and h_1 is narrower than that of m_2 and h_2, since the SPANDAR refractivity profile can be well approximated by a bilinear function.

[39] The average measured refractivity along the first 55 km of recordings and 150° azimuth, the observed clutter along the same angle, and the distribution of clutter power between azimuth 145–155° are compared to the inverted trilinear profiles and their modeled clutter in Figures 7b and 7c. Figure 7b shows that the refractivity profile estimated from the multiple angle clutter model has the closest resemblance to the average refractivity profile measured by the helicopter.

[40] Another important characteristic of refractivity profiles is the M-deficit, which is defined as the total change in the modified refractivity of the trapping layer. The average M-deficit of the observed profile from 0 to 55 km is 22 M-units. This is consistent with the inverted profile with 20 M-units of M-deficit, using the multiple angle clutter model.

[41] Previous RFC studies that used the 1998 SPANDAR data set were based on an angle-independent clutter model for inversions. Although results of Figure 7 suggests that the multiple clutter model is a better model for inverting clutter data for estimating refractivity profiles, more analysis with real data is required for verification.

4. Conclusion

[42] RFC estimates the refractivity profile of maritime environments from observed radar clutter. A grazing angle independent clutter model was assumed in previous studies. Two new clutter models are considered here: a range-dependent multiple angle clutter model and a range-dependent single angle clutter model based on the maximum grazing angle from ray theory. Multiple angle clutter includes all incident grazing angles weighted proportional to their relative powers at each range.

[43] The performance of clutter models in RFC is compared in a simulated surface-based duct, a range-dependent evaporation duct, and the 1998 SPANDAR data set. The differences in the clutter power of different models are projected into the environmental parameter domain during the RFC inversion. Results show that the range-dependent single angle clutter model based on the maximum grazing angle yields biased estimations relative to the multiple angle clutter model. An angle-independent clutter model also yields biased parameter inversions, especially when inverting for range-dependent refractivity profiles. Although more analysis is required, the results suggest that the multiple angle clutter model yields more accurate RFC inversions, especially when surface-based ducts and range varying environments are present.

[44] **Acknowledgments.** This work was supported by SPAWAR under grants N66001-03-2-8938, TDL 0049 and TDL 0054.

References

Barrios, A. E. (1994), A terrain parabolic equation model for propagation in the troposphere, *IEEE Trans. Antennas Propag.*, *42*(1), 90–98, doi:10.1109/8.272306.

Barrios, A. E. (2002), Advanced propagation model (APM) computer software configuration item (CSCI), *TD 3145*, Space and Nav. Warfare Syst. Cent., San Diego, Calif.

Dockery, G. D. (1988), Modeling electromagnetic wave propagation in the troposphere using the parabolic equation, *IEEE Trans. Antennas Propag.*, *36*(10), 1464–1470, doi:10.1109/8.8634.

Dockery, G. D. (1990), Method for modeling sea surface clutter in complicated propagation environments, *IEE Proc. Radar Signal Process.*, *137*, 73–79.

Dockery, G. D., R. S. Awadallah, D. E. Freund, J. Z. Gehman, and M. H. Newkirk (2007), An overview of recent advances for the TEMPER radar propagation model, in *IEEE Radar Conference*, pp. 896–905, Inst. of Electr. and Electron. Eng., New York.

Douvenot, R., and V. Fabbro (2010), On the knowledge of radar coverage at sea using real time refractivity from clutter, *IET Radar Sonar Navig.*, *4*(2), 293–301, doi:10.1049/iet-rsn.2009.0073.

Douvenot, R., V. Fabbro, P. Gerstoft, C. Bourlier, and J. Saillard (2010), Real time refractivity from clutter using a best fit approach improved with physical information, *Radio Sci.*, *45*, RS1007, doi:10.1029/2009RS004137.

Gerstoft, P., L. T. Rogers, J. L. Krolik, and W. S. Hodgkiss (2003), Inversion for refractivity parameters from radar sea clutter, *Radio Sci.*, *38*(3), 8053, doi:10.1029/2002RS002640.

Gregers-Hansen, V., and R. Mital (2009), An empirical sea clutter model for low grazing angles, in *IEEE Radar Conference*, pp. 1–5, Inst. of Electr. and Electron. Eng., New York.

Horst, M., F. Dyer, and M. Tuley (1978), Radar sea clutter model, in *Proceedings of the International IEEE AP/S URSI Symposium, Part 2*, pp. 6–10, Inst. of Electr. and Electron. Eng., New York.

Karimian, A., C. Yardim, P. Gerstoft, W. S. Hodgkiss, and A. E. Barrios (2011), Refractivity estimation from sea clutter: An invited review, *Radio Sci.*, *46*, RS6013, doi:10.1029/2011RS004818.

Kerr, D. E. (1951), *Propagation of Short Radio Waves*, McGraw-Hill, New York.

LeFurjah, G., R. Marshall, T. Casey, T. Haack, and D. De Forest Boyer (2010), Synthesis of mesoscale numerical weather prediction and empirical site-specific radar clutter models, *IET Radar Sonar Navig.*, *4*(6), 747–754.

Levy, M. (2000), *Parabolic Equation Methods for Electromagnetic Wave Propagation*, Inst. of Electr. Eng., London.

Long, M. W. (2000), *Radar Reflectivity of Land and Sea*, 3rd ed., Artech House, Norwood, Mass.

Lowry, A. R., C. Rocken, S. V. Sokolovskiy, and K. D. Anderson (2002), Vertical profiling of atmospheric refractivity from ground-based GPS, *Radio Sci.*, *37*(3), 1041, doi:10.1029/2000RS002565.

Patterson, W. (1992), Ducting climatology summary, technical report, Space and Nav. Warfare Syst. Cent., San Diego, Calif.

Paulus, R. A. (1985), Practical applications of an evaporation duct model, *Radio Sci.*, *20*, 887–896, doi:10.1029/RS020i004p00887.

Reilly, J. P., and G. D. Dockery (1988), Calculation of radar sea return with consideration of propagation conditions, *AAW Tech. Rep. NNW-88-141*, NATO, Brussels.

Rogers, L. T. (1997), Likelihood estimation of tropospheric duct parameters from horizontal propagation measurements, *Radio Sci.*, *32*, 79–92, doi:10.1029/96RS02904.

Rogers, L. T., C. P. Hattan, and J. K. Stapleton (2000), Estimating evaporation duct heights from radar sea echo, *Radio Sci.*, *35*(4), 955–966, doi:10.1029/1999RS002275.

Rogers, L. T., M. Jablecki, and P. Gerstoft (2005), Posterior distributions of a statistic of propagation loss inferred from radar sea clutter, *Radio Sci.*, *40*, RS6005, doi:10.1029/2004RS003112.

Rowland, J. R., G. C. Konstanzer, M. R. Neves, R. E. Miller, J. H. Meyer, and J. R. Rottier (1996), Seawasp: Refractivity characterization using shipboard sensors, in *Battlespace Atmospheric Conferene*, pp. 155–164, RDT&E Div., Nav. Command Control and Ocean Surv. Cent., San Diego, Calif.

Skolnik, M. I. (2008), *Radar Handbook*, 3rd ed., McGraw-Hill, New York.

Someda, C. G. (2006), *Electromagnetic Waves*, 2nd ed., CRC Press, Boca Raton, Fla.

Vasudevan, S., R. H. Anderson, S. Kraut, P. Gerstoft, L. T. Rogers, and J. L. Krolik (2007), Recursive Bayesian electromagnetic refractivity estimation from radar sea clutter, *Radio Sci.*, *42*, RS2014, doi:10.1029/2005RS003423.

Ward, K. D., R. J. A. Tough, and S. Watts (2005), *Sea Clutter: Scattering, the K Distribution and Radar Performance*, Inst. of Eng. and Technol., London.

Willitsford, A., and C. R. Philbrick (2005), Lidar description of the evaporative duct in ocean environments, *Proc, SPIE*, *5885*, 140–147.

Yardim, C., P. Gerstoft, and W. S. Hodgkiss (2006), Estimation of radio refractivity from radar clutter using Bayesian Monte Carlo analysis, *IEEE Trans. Antennas Propag.*, *54*(4), 1318–1327, doi:10.1109/TAP.2006.872673.

Yardim, C., P. Gerstoft, and W. S. Hodgkiss (2007), Statistical maritime radar duct estimation using hybrid genetic algorithm–Markov chain Monte Carlo method, *Radio Sci.*, *42*, RS3014, doi:10.1029/2006RS003561.

Yardim, C., P. Gerstoft, and W. S. Hodgkiss (2008), Tracking refractivity from clutter using Kalman and particle filters, *IEEE Trans. Antennas Propag.*, *56*(4), 1058–1070, doi:10.1109/TAP.2008.919205.

Yardim, C., P. Gerstoft, and W. S. Hodgkiss (2009), Sensitivity analysis and performance estimation of refractivity from clutter techniques, *Radio Sci.*, *44*, RS1008, doi:10.1029/2008RS003897.

A. E. Barrios, Atmospheric Propagation Branch, Space and Naval Warfare Systems Center, San Diego, CA 92152-7385, USA. (amalia.barrios@navy.mil)

P. Gerstoft, W. S. Hodgkiss, A. Karimian, and C. Yardim, Marine Physical Laboratory, Scripps Institution of Oceanography, University of California, San Diego, La Jolla, CA 92037-0238, USA. (gerstoft@ucsd.edu; whodgkiss@ucsd.edu; akarimian@ucsd.edu; cyardim@ucsd.edu)